no further increase in infection (Fig. 4G and fig. S12), suggesting that the effects of BADGE on cathelicidin production from adipocytes was responsible for the increase in *S. aureus* infection in vivo.

These results show that a local increase in subcutaneous adipocytes is an important host defense response against skin infection. This observation is consistent with prior observations that adipocytes secrete a variety of bioactive adipokines and cytokines that mediate immune responses after injury (*28*) and now shows that adipocytes produce an AMP that can directly kill bacteria. Local expansion of dermal fat produces cathelicidin in response to infection, but this response appears to decline as adipocytes mature. The expansion of dermal fat in response to infection may also indirectly benefit immune defense by influencing other processes such as neutrophil oxidative burst, thus further amplifying the importance of the subcutaneous preadipocyte pool in preventing infections. Defective AMP production by mature adipocytes may explain observations of elevated susceptibility to infection during obesity and insulin resistance (*29*). Cathelicidin has also been shown to be proinflammatory (*30*). Therefore, the production of cathelicidin by adipocytes may also participate in the chronic, low-level inflammation observed in obesity (*28*).

REFERENCES AND NOTES

1. F. O. Nestle, P. Di Meglio, J. Z. Qin, B. J. Nickoloff, *Nat. Rev. Immunol.* **9**, 679–691 (2009).
2. R. L. Gallo, L. V. Hooper, *Nat. Rev. Immunol.* **12**, 503–516 (2012).
3. V. Nizet *et al.*, *Nature* **414**, 454–457 (2001).
4. P. Y. Ong *et al.*, *N. Engl. J. Med.* **347**, 1151–1160 (2002).
5. K. Pütsep, G. Carlsson, H. G. Boman, M. Andersson, *Lancet* **360**, 1144–1149 (2002).
6. L. S. Miller, J. S. Cho, *Nat. Rev. Immunol.* **11**, 505–518 (2011).
7. J. M. Musser *et al.*, *Proc. Natl. Acad. Sci. U.S.A.* **87**, 225–229 (1990).
8. J. Eguchi *et al.*, *Cell Metab.* **13**, 249–259 (2011).
9. H. S. Sul, *Mol. Endocrinol.* **23**, 1717–1725 (2009).
10. C. S. Hudak *et al.*, *Cell Reports* **8**, 678–687 (2014).
11. R. K. Gupta *et al.*, *Nature* **464**, 619–623 (2010).
12. T. Tanaka, N. Yoshida, T. Kishimoto, S. Akira, *EMBO J.* **16**, 7432–7443 (1997).
13. M. I. Lefterova *et al.*, *Genes Dev.* **22**, 2941–2952 (2008).
14. E. Festa *et al.*, *Cell* **146**, 761–771 (2011).
15. W. A. Alcaraz *et al.*, *Proc. Natl. Acad. Sci. U.S.A.* **103**, 19424–19429 (2006).
16. L. E. Cheng, J. Zhang, R. R. Reed, *Dev. Biol.* **307**, 43–52 (2007).
17. R. K. Gupta *et al.*, *Cell Metab.* **15**, 230–239 (2012).
18. R. R. Driskell *et al.*, *Nature* **504**, 277–281 (2013).
19. O. Naveiras *et al.*, *Nature* **460**, 259–263 (2009).
20. B. A. Schmidt, V. Horsley, *Development* **140**, 1517–1527 (2013).
21. H. Green, O. Kehinde, *Cell* **5**, 19–27 (1975).
22. R. A. Dorschner *et al.*, *J. Invest. Dermatol.* **117**, 91–97 (2001).
23. T. Sillat *et al.*, *J. Cell. Mol. Med.* **16**, 1485–1495 (2012).
24. O. E. Sørensen *et al.*, *Blood* **97**, 3951–3959 (2001).
25. O. E. Sørensen *et al.*, *J. Biol. Chem.* **278**, 28540–28546 (2003).
26. N. Kawaguchi *et al.*, *Am. J. Pathol.* **160**, 1895–1903 (2002).
27. H. G. Boman, *J. Intern. Med.* **254**, 197–215 (2003).
28. A. Schäffler, J. Schölmerich, *Trends Immunol.* **31**, 228–235 (2010).
29. W. P. Cawthorn, E. L. Scheller, O. A. MacDougald, *J. Lipid Res.* **53**, 227–246 (2012).
30. K. Yamasaki *et al.*, *Nat. Med.* **13**, 975–980 (2007).

ACKNOWLEDGMENTS

This study was supported by NIH R01 AI083358, R01AI052453, and AR052728 (R.L.G.). Human serum collections were funded by The Atopic Dermatitis Research Network (HHSN272201000020C). S.P.B. was supported by the NIH (DK096828). M.V.P. is supported by the Edward Mallinckrodt Jr. Foundation Research Grant, the Dermatology Foundation Research Grant, and NIH NIAMS R01-AR067273; C.F.G.-J. is supported by the NIH MBRS-IMSD training grant (GM055246) and NSF Graduate Research Fellowship number DGE-1321846; and R.R. is supported by California Institute for Regenerative Medicine training grant (TG2-01152). The authors declare no competing financial interests. We thank T. Nakatuji for advice relating to bacterial infections and C. Aguilera for mouse technical expertise, UCSD Bio-Core facility for reagents, UCSD mouse hematology core laboratory for serum studies, and J. M. Olefsky for comments on the manuscript. Zfp423-GFP mice are available from R. Gupta under a material transfer agreement with Dana-Farber Cancer Institute. All the data reported in this manuscript are presented in the main paper and in the supplementary materials.

SUPPLEMENTARY MATERIALS

www.sciencemag.org/content/347/6217/67/suppl/DC1
Materials and Methods
Figs. S1 to S12
Table S1
References (*31*–*37*)

8 September 2014; accepted 21 November 2014
10.1126/science.1260972

VIRUS STRUCTURE

Structure and inhibition of EV-D68, a virus that causes respiratory illness in children

Yue Liu,[1] Ju Sheng,[1] Andrei Fokine,[1] Geng Meng,[1] Woong-Hee Shin,[1] Feng Long,[1] Richard J. Kuhn,[1] Daisuke Kihara,[1,2] Michael G. Rossmann[1]*

Enterovirus D68 (EV-D68) is a member of *Picornaviridae* and is a causative agent of recent outbreaks of respiratory illness in children in the United States. We report here the crystal structures of EV-D68 and its complex with pleconaril, a capsid-binding compound that had been developed as an anti-rhinovirus drug. The hydrophobic drug-binding pocket in viral protein 1 contained density that is consistent with a fatty acid of about 10 carbon atoms. This density could be displaced by pleconaril. We also showed that pleconaril inhibits EV-D68 at a half-maximal effective concentration of 430 nanomolar and might, therefore, be a possible drug candidate to alleviate EV-D68 outbreaks.

Picornaviruses constitute a large family of small icosahedral viruses with a single positive-stranded RNA genome and an external diameter of about 300 Å. The *Enterovirus* genus includes medically important human pathogens, such as human rhinoviruses (HRVs), polioviruses (PVs) and coxsackieviruses (CVs) (table S1) (*1*, *2*). Many of these enteroviruses (EVs) have been well characterized structurally and functionally (*3*–*10*). However, the species EV-D remains poorly characterized.

An upsurge of EV-D68 cases in the past few years has shown clusters of infections worldwide (*11*). In August 2014, an outbreak of mild to severe respiratory illnesses occurred among thousands of young children in the United States, of which 1116 cases have been confirmed to be caused by EV-D68. This virus has also been associated with occasional neurological infections (*12*). Although EV-D68 has emerged as a considerable global public health threat, there is no available vaccine or effective antiviral treatment.

The capsids of EVs consist of 60 copies of each of four different viral proteins: VP1, VP2, VP3, and VP4 (Fig. 1A). Of these, VP1 (about 300 amino acids), VP2 (about 260 amino acids), and VP3 (about 240 amino acids) each have a "jelly roll" fold arranged in the capsid with pseudo $T = 3$ icosahedral symmetry, where T represents the triangulation number (*13*). Their organization in the capsid is similar to that of the $T = 3$ RNA plant viruses, except that the three subunits related by quasi-threefold symmetry have different amino acid sequences in picornaviruses (*6*, *10*). Each roughly 70–amino–acids-long VP4 molecule forms an extended peptide on the internal surface of the capsid shell. The jelly roll fold consists of two antiparallel β sheets, which face each other to form a β barrel with a hydrophobic interior (Fig. 1B).

EVs have a deep surface depression ("canyon") circulating around each of the 12 pentameric vertices (Fig. 1A). The canyon was predicted to be the site of receptor binding, because the amino acids outside the canyon that form the external surface of the virus were more exposed and were shown to be accessible to neutralizing antibodies (Fig. 1A) (*10*, *14*). The virus thus could remain faithful to a specific receptor molecule that binds into the canyon while evading the host's immune system (*10*, *15*). The prediction that the canyon would be the site of binding to cellular receptor molecules was subsequently confirmed for numerous different EVs (*16*, *17*). All of the receptor

[1]Department of Biological Sciences, Hockmeyer Hall of Structural Biology, 240 South Martin Jischke Drive, Purdue University, West Lafayette, IN 47907, USA. [2]Department of Computer Science, 305 North University Street, Purdue University, West Lafayette, IN 47907, USA.
***Corresponding author. E-mail: mr@purdue.edu**

molecules were found to have an immunoglobulin-like structure.

A variety of small ~350-dalton hydrophobic molecules that are inhibitors of EV infection were shown to bind into the hydrophobic pocket in the center of the VP1 jelly roll (*18*) (Fig. 1B). They stabilize the virus (*19*) by filling the pocket with a well-fitting hydrophobic molecule, thereby inhibiting uncoating of the virus and the release of the genome into the infected cell. These compounds also prevent viral attachment to cells by altering the surface features of the canyon floor, where the virus attaches to a cellular receptor (*17*, *19*). The floor of the canyon is formed primarily by the GH loop of VP1, the connecting residues between β-strands G and H (*18*).

Most infectious EVs contain a small molecule or "pocket factor," probably a fatty acid in the VP1 binding pocket (*7*, *18*, *20*). Like the capsid-binding compounds, the pocket factor presumably stabilizes the virus by filling the VP1 hydrophobic pocket. Thus, the virus is stabilized while being transmitted to a new host. However, when a receptor molecule binds to the floor of the canyon, it depresses the floor (that also forms the roof of the VP1 binding pocket), which then squeezes the binding pocket, probably expelling the pocket factor (*17*). Thus, the attachment of the virus to a cell surface initiates uncoating, causing the release of the viral genome into the cell's cytosol.

In most EVs that have been investigated, these capsid-binding antiviral compounds displace the pocket factor (e,g. polioviruses, coxsackieviruses A or B, and many HRVs). The rhinoviruses HRV14 (*18*) and HRV3 (*21*) do not contain a pocket factor, and the GH loop is displaced relative to its position in other EVs that contain a pocket factor, reducing the volume of the VP1 pocket. Either neither HRV14 nor HRV3 binds a pocket factor in vivo or it was lost during the purification procedure. Much effort was made between 1985 and 2000 to design a compound that fits into the VP1 pocket and would inhibit the maximum number of rhinovirus serotypes (*22*). The final optimal structure was pleconaril (fig. S1), which not only had good efficacy but was also stable enough to maintain good bioavailability in clinical tests (*23*). However, pleconaril was not licensed, primarily because it put women using birth control drugs at risk of conception.

The EV-D68 prototype strain Fermon CA62-1 was propagated in human rhabdomyosarcoma cells at 33°C, which had previously been shown to be the optimal growth temperature for EV-D68, indicating that EV-D68 behaves much like members of the RV-A and RV-B species that are responsible for common colds (*24*). The virus was purified and crystalized as described in the supplementary materials and methods. The cubic-looking crystals had a diameter between 0.1 and 0.2 mm. After soaking in glycerol, they were flash-frozen in liquid nitrogen. X-ray diffraction data were collected at sector 14 of the Advanced Photon Source. The data extended to 2.0 Å resolution and were processed with HKL2000 (*25*). The crystal symmetry was I222, with two particles per unit cell, implying that the particles were located on a 222 symmetry position. A rotation function (*26*) differentiated between the two orthogonal possible orientations of the icosahedron. Initial phases were calculated based on the structure of HRV2 (*27*) (Protein Data Bank accession number 1FPN) after the pocket factor was removed. The phases were then extended in small steps to 2.0 Å resolution, using 15-fold averaging and solvent flattening. A model of the structure was built using the program Coot (*28*) and refined with the program CNS (*29*). The final value of R_{work} was 27.5%. R_{free} is essentially the same as R_{work} in the presence of high noncrystallographic symmetry redundancy as is the case here (table S2).

Comparison of the amino acid sequences of EV-D68 with those of other EVs shows that VP3 has a short C-terminal α helix not present in other EVs (fig. S2). The EV-D68 electron density map showed that this helix decorates the north side of the canyon in the neighboring, fivefold-related, icosahedral asymmetric unit. As a result, the canyon is narrower than in other EVs and might therefore not be large enough to accommodate immunoglobulinlike receptors (Fig. 1C).

The BC and DE loops of VP1 are structurally the most variable among known picornaviruses. The EV-D68 VP1 has two disordered regions corresponding to residues 80 to 86 (EV-D68 numbering) in the BC loop and 129 to 136 in the DE loop, both of which are near fivefold axes. These regions harbor the neutralizing immunogen sites NIm-IA and NIm-IB on HRV14, respectively (*10*) (Fig. 1A). Thus the flexible immunogenic regions around the fivefold axes might be an alternative mechanism for evading host humoral immune responses.

The electron density map of EV-D68 showed density in the VP1 pocket (Fig. 2A). The height of this pocket factor density was about three standard deviations above the mean of the noncrystallographic symmetry averaged map, as compared with about five standard deviations of most of the main-chain density. As in other EVs that have a pocket factor, the conformation of the GH loop of VP1, which defines the interface between the VP1 pocket and the floor of the canyon, is pushed into the canyon relative to the empty pocket in HRV14 (*10*, *18*) or HRV3 (*21*).

The length of the pocket factor density in the EV-D68 map corresponded to a fatty acid with an aliphatic chain of about 10 carbon atoms (Fig. 2B). Similarly, 12–carbon-atom-long pocket factors were observed for HRV16 (*9*) and HRV2 (*27*). In contrast, the well-formed pocket factors in poliovirus 1 (*6*, *7*), coxsackievirus B3 (*5*), and EV-A71 (*3*) corresponded to longer fatty acids with 18, 16, and 18 carbon atoms, respectively. Furthermore, the orientation of the pocket factor

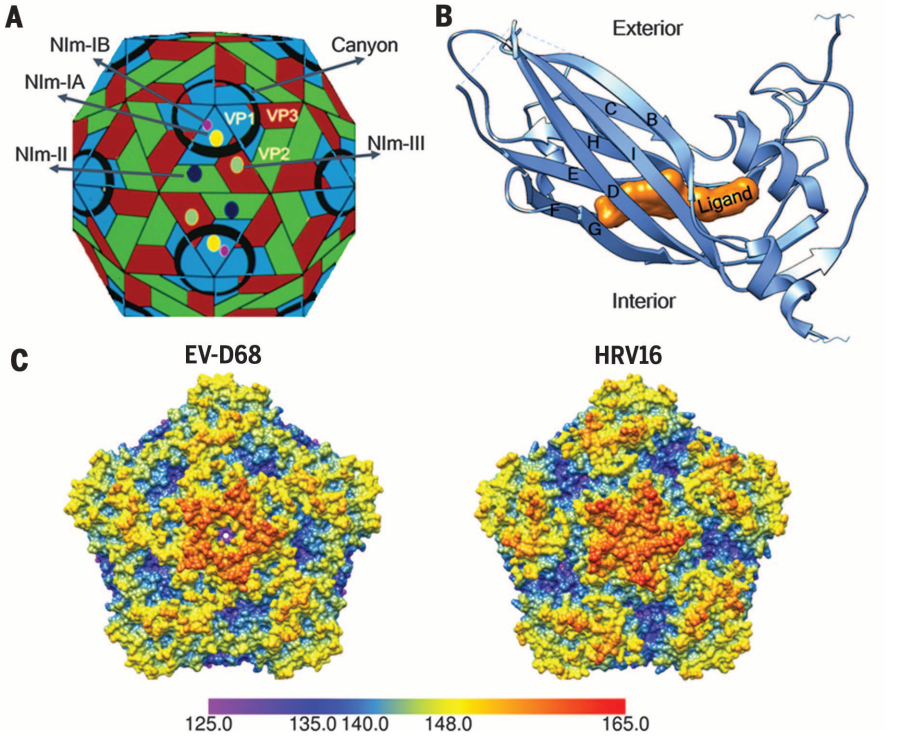

Fig. 1. The structure of EV-D68. (**A**) Diagrammatic representation of the virus. VP1, VP2, and VP3 are colored blue, green, and red, respectively. Each pentagonal icosahedral vertex is surrounded by a canyon colored black. The epitopes for neutralizing antibodies for the homologous HRV14 are labeled as NIm-I, NIm-II, and NIm-III. The NIm-IA and NIm-IB sites are disordered in EV-D68. (**B**) The VP1 jelly roll in EV-D68 shown as a ribbon diagram. If the β strands along the polypeptide are identified sequentially as A, B, C,….I, then one of the sheets is composed of the antiparallel strands BIDG and the other by the antiparallel strands CHEF. (**C**) Surface features of EV-D68 compared to HRV16. The canyon of EV-D68 is shallower and narrower than the canyon of HRV16.

tails in EV-D68, HRV16, and HRV2 is slightly different than that of the long pocket factors of EV-A71, poliovirus 1, and coxsackievirus B3 (Fig. 2C). The orientation is controlled in part by VP1 residue 184, which is Leu or Ile for the viruses with small, short pocket factors and Val for viruses with longer pocket factors (fig. S2). The larger Leu or Ile residue pushes the pocket factor sideways. The similarity between the properties of the pocket factor in EV-D68 and that in the HRVs might partially explain why these viruses are less stable.

The anti–EV-D68 activity of two capsid-binding compounds, pirodavir and BTA-188 (fig. S1), that had significant anti-rhinovirus activity was compared with pleconaril, using plaque reduction assays in HeLa cells (Fig. 3, A and B). The half-maximal effective concentration (EC_{50}) value of these two compounds was found to be comparable to previous results using cytopathic effect inhibition assays against EV-D68 (*30*). However, pleconaril was found to be more potent against EV-D68 than pirodavir and BTA-188 (Fig. 3A). The inhibitory effect of pleconaril is similar against EV-D68, HRV16, and HRV14, but better than against EV-A71. It is therefore noteworthy that pleconaril was an effective inhibitor in extensive clinical tests for the treatment of common colds (*23*, *31*). Furthermore, fluorescence-based thermal stability assays indicated that when EV-D68 was incubated with pleconaril at either 10 or 50 μg/ml, 4°C higher temperatures were required to release the RNA genome than when no pleconaril was present (Fig. 3C and materials and methods in the supplementary materials). Thus, pleconaril stabilizes EV-D68 capsids, preventing the virus from uncoating during viral entry.

The structure of EV-D68 was also determined to 2.3 Å resolution when co-crystalized with pleconaril (fig. S3). The crystallographic procedure was the same as for the native structure determination (materials and methods in the supplementary materials). The electron density of the ligand inside the hydrophobic pocket was of the same height but much longer than that of the pocket factor in the native EV-D68 structure (Fig. 4A) and could be easily fitted with the structure of pleconaril (Fig. 4B). This demonstrated that the native pocket factor was replaced by pleconaril. However, the densities of the ligand and of the pocket factor are slightly lower than that of the polypeptide main chain. In part this is to be expected, because the ligand or fatty acid pocket factor is composed primarily of only carbon atoms as opposed to the heavier combination of carbon and nitrogen plus oxygen atoms of the main chain. In part, the slightly lower density of the ligand might be due to some variations of conformation within the VP1 binding pocket.

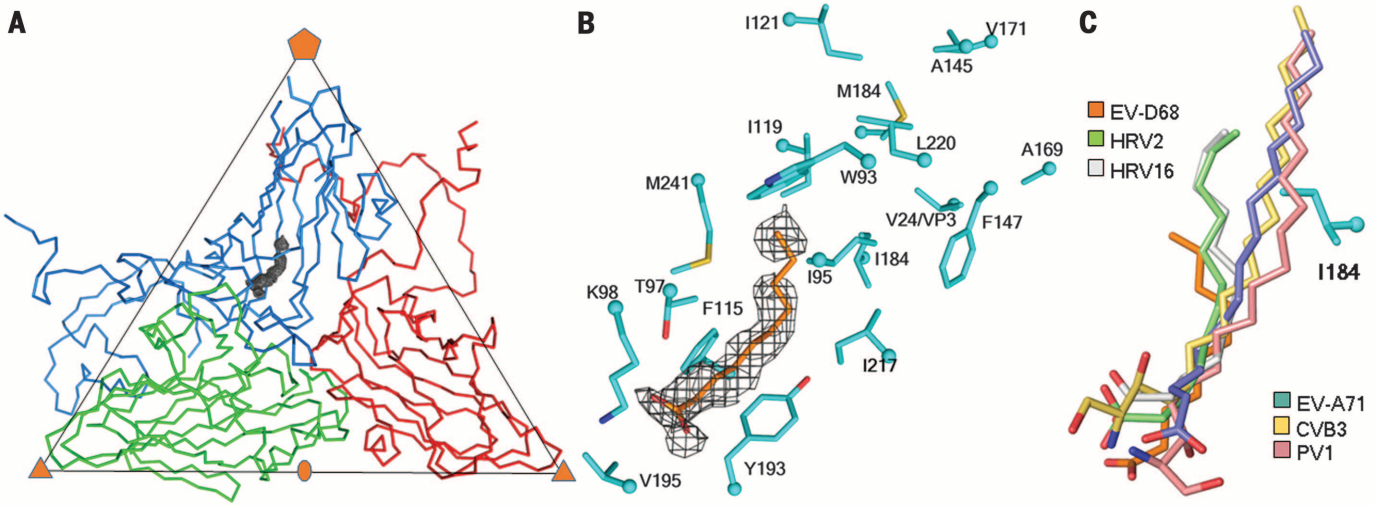

Fig. 2. The pocket factor. (**A**) One icosahedral asymmetric unit of the EV-D68 structure, showing the Cα atom backbone for VP1, VP2, and VP3 in marine blue, green, and red, respectively. The pocket factor electron density outline is shown in gray. (**B**) Enlargement of the pocket factor density with a fitted putative C10 fatty acid. Shown also are the amino acids lining the pocket. (**C**) Comparison of the putative pocket factor structures in six known EV structures. Shown also is the residue I184 in EV-D68 that alters the direction of the shorter pocket factors in some of the viruses as compared to others with longer pocket factors and a smaller residue at the equivalent position of 184. Atoms at the head of the pocket factors and of the VP1 residue side chains are colored red (oxygen), dark blue (nitrogen), and yellow (sulfur).

A

Anti-enterovirus activity of three compounds

Virus	EC_{50} (μM)		
	Pleconaril	Pirodavir	BTA-188
EV-D68	0.43±0.02*	1.61±0.30*	>4.93*
EV-D68	-†	2.44±0.54‡	3.34±0.08‡
HRV16	0.57§	0.016±0.034‡	0.008±0.002‡
HRV14	0.16§	0.027±0.043‡	0.068±0.033‡
EV-A71	>262‖	5.42±0.49‡	0.082±0.139‡

*Data were reported in this work
†No reported data were available
‡According to Barnard et al. (2004) *(30)*
§According to Ledford et al. (2004) *(32)*
‖According to Tijsma et al. (2014) *(33)*

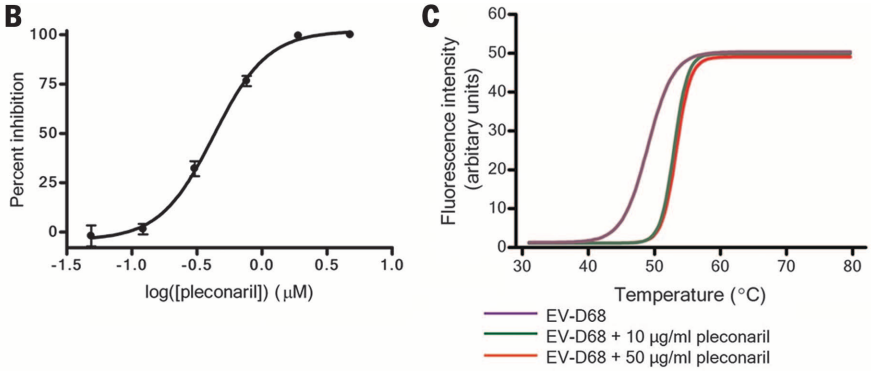

Fig. 3. Anti-EV activity of three capsid-binding compounds. (**A**) List of EC_{50} values (*30*, *32*, *33*). Each experiment was performed at least three times. (**B**) Plot of the percent of plaque reduction of pleconaril as a function of the log of its concentration. Error bars indicate standard deviations. (**C**) Release of EV-D68 genome upon increase in temperature as monitored by Sybr green II. The experiments were done in triplicate. For each data point, the ratio between mean fluorescence intensity and standard deviation is at least 7.6. Shown are curves fitted with a sigmoidal function for the native virus and for the virus after incubation with pleconaril.

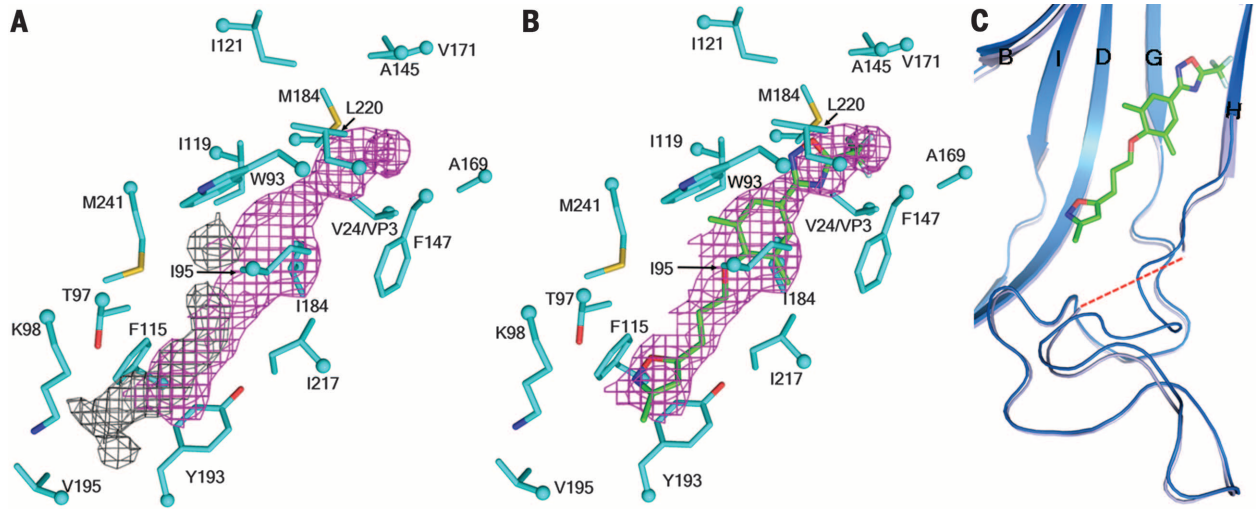

Fig. 4. Structure of pleconaril bound into the VP1 pocket of EV-D68. (**A**) Pocket factor density (gray) compared to the pleconaril density (magenta). (**B**) Pleconaril (green) fitted to density in the structure of the complex. (**C**) Conformational change of the VP1 GH loop as a consequence of the presence of pleconaril. The native and complex structures are shown in marine blue and baby blue, respectively. Oxygen, nitrogen, sulfur, and fluorine atoms are shown in red, dark blue, yellow, and light green, respectively.

Part of the VP1 GH loop (residues 212 to 215) that forms the entrance to the VP1 pocket had become less ordered in the EV-D68-pleconaril complex. The Cα atom of residue 211 had moved 1.2 Å toward the inside of the pocket relative to that of the native structure, possibly blocking the entrance to the pocket once pleconaril had entered (Fig. 4C). Thus, the dynamics of the GH loop might be a consideration for future structure-based design of EV-D68 capsid-binding inhibitors.

A comparison of the EV-D68–pleconaril, HRV14-pleconaril, and HRV16-pleconaril structures showed a similar binding mode for pleconaril in the VP1 pocket of these three viruses (fig. S4 and table S3). This may explain why pleconaril is similarly effective against these three EVs. To investigate why pleconaril is more effective against EV-D68 than pirodavir or BTA-188, we performed in silico docking experiments. The presence of a trifluoromethyl-substituted oxadiazole moiety in pleconaril, rather than a more hydrophilic group in either pirodavir (ethyl carboxylate group) or BTA-188 (O-ethyloxime group) at structurally equivalent positions (fig. S5), probably contributes to more favorable interactions of pleconaril with the hydrophobic residues deep inside the VP1 pocket of EV-D68.

Our results show that the structure of EV-D68 has considerable similarities to those of the well-studied HRVs for which pleconaril was specifically designed. We also show that pleconaril replaces the pocket factor and is a potent inhibitor of EV-D68, with an EC_{50} value of 430 nM. The size and location of the pocket factor lodged in the VP1 pocket are similar to those found in other HRVs and different from those of the pocket factors found in poliovirus 1 and EV-A71. This correlates with the observation that pleconaril is far more active when the natural pocket factor is short, as in the HRVs and in EV-D68. Furthermore, sequence alignment of 188 EV-D68 strains found between 1962 and 2013 indicates that residues in VP1 that interact with pleconaril, as identified from the complex structure, are completely conserved, with one exception. Therefore, pleconaril is likely to inhibit not only the prototype strain examined here but also many other strains. In view of the previous extensive clinical trials that have established its safety, pleconaril would be a possible drug candidate to alleviate EV-D68 outbreaks.

REFERENCES AND NOTES

1. M. J. Adams, A. M. King, E. B. Carstens, *Arch. Virol.* **158**, 2023–2030 (2013).
2. N. J. Knowles *et al.*, in *Virus Taxonomy: Classification and Nomenclature of Viruses: Ninth Report of the International Committee on Taxonomy of Viruses*, A. M. Q. King, M. J. Adams, E. B. Carstens, E. J. Lefkowitz, Eds. (Elsevier, San Diego, CA, 2012), pp. 855–880.
3. P. Plevka, R. Perera, J. Cardosa, R. J. Kuhn, M. G. Rossmann, *Science* **336**, 1274 (2012).
4. X. Wang *et al.*, *Nat. Struct. Mol. Biol.* **19**, 424–429 (2012).
5. J. K. Muckelbauer *et al.*, *Structure* **3**, 653–667 (1995).
6. J. M. Hogle, M. Chow, D. J. Filman, *Science* **229**, 1358–1365 (1985).
7. D. J. Filman *et al.*, *EMBO J.* **8**, 1567–1579 (1989).
8. K. N. Lentz *et al.*, *Structure* **5**, 961–978 (1997).
9. M. A. Oliveira *et al.*, *Structure* **1**, 51–68 (1993).
10. M. G. Rossmann *et al.*, *Nature* **317**, 145–153 (1985).
11. R. Tokarz *et al.*, *J. Gen. Virol.* **93**, 1952–1958 (2012).
12. J. D. Kreuter *et al.*, *Arch. Pathol. Lab. Med.* **135**, 793–796 (2011).
13. D. L. Caspar, A. Klug, *Cold Spring Harbor Symp. Quant. Biol.* **27**, 1–24 (1962).
14. B. Sherry, A. G. Mosser, R. J. Colonno, R. R. Rueckert, *J. Virol.* **57**, 246–257 (1986).
15. M. G. Rossmann, *J. Biol. Chem.* **264**, 14587–14590 (1989).
16. N. H. Olson *et al.*, *Proc. Natl. Acad. Sci. U.S.A.* **90**, 507–511 (1993).
17. M. G. Rossmann, Y. He, R. J. Kuhn, *Trends Microbiol.* **10**, 324–331 (2002).
18. T. J. Smith *et al.*, *Science* **233**, 1286–1293 (1986).
19. M. G. Rossmann, *Protein Sci.* **3**, 1712–1725 (1994).
20. M. Smyth, T. Pettitt, A. Symonds, J. Martin, *Arch. Virol.* **148**, 1225–1233 (2003).
21. R. Zhao *et al.*, *Structure* **4**, 1205–1220 (1996).
22. J. M. Rogers, G. D. Diana, M. A. McKinlay, *Adv. Exp. Med. Biol.* **458**, 69–76 (1999).
23. F. G. Hayden *et al.*, *Clin. Infect. Dis.* **36**, 1523–1532 (2003).
24. M. S. Oberste *et al.*, *J. Gen. Virol.* **85**, 2577–2584 (2004).
25. Z. Otwinowski, W. Minor, *Methods Enzymol.* **276**, 307–326 (1997).
26. L. Tong, M. G. Rossmann, *Methods Enzymol.* **276**, 594–611 (1997).
27. N. Verdaguer, D. Blaas, I. Fita, *J. Mol. Biol.* **300**, 1179–1194 (2000).
28. P. Emsley, B. Lohkamp, W. G. Scott, K. Cowtan, *Acta Crystallogr. D Biol. Crystallogr.* **66**, 486–501 (2010).
29. A. T. Brünger *et al.*, *Acta Crystallogr. D Biol. Crystallogr.* **54**, 905–921 (1998).
30. D. L. Barnard *et al.*, *Antimicrob. Agents Chemother.* **48**, 1766–1772 (2004).
31. D. C. Pevear *et al.*, *Antimicrob. Agents Chemother.* **49**, 4492–4499 (2005).
32. R. M. Ledford *et al.*, *J. Virol.* **78**, 3663–3674 (2004).
33. A. Tijsma *et al.*, *Antimicrob. Agents Chemother.* **58**, 6990–6992 (2014).

ACKNOWLEDGMENTS

We thank M. Steven Oberste of the Centers for Disease Control and Prevention for supplying us with the prototype strain of EV-D68; M. A. McKinlay of the Task Force for Global Health for helpful discussion and suggestions; S. Kelly for help with the manuscript preparation; and V. Srajer, R. Henning, and the other staff of the Advanced Photon Source BioCARS beamline 14 for help with x-ray diffraction data collection. Use of BioCARS sector 14 was supported by the National Institutes of Health, National Center for Research Resources (NIH/NCRR) grant RR007707. Use of the Advanced Photon Source was supported by the U.S. Department of Energy, Office of Science, Office of Basic Energy Sciences, under contract DE-AC02-006CH11357. This study was supported by NIH grant award AI11219 to M.G.R. Coordinates for native EV-D68 and EV-D68–pleconaril structures were deposited with the Protein Data Bank with accession numbers 4WM8 and 4WM7, respectively.

SUPPLEMENTARY MATERIALS

www.sciencemag.org/content/347/6217/71/suppl/DC1
Materials and Methods
Figs. S1 to S5
Tables S1 to S3
References (*34*–*49*)

1 October 2014; accepted 25 November 2014
10.1126/science.1261962

Structure and inhibition of EV-D68, a virus that causes respiratory illness in children

Yue Liu *et al.*

Science **347**, 71 (2015);
DOI: 10.1126/science.1261962

Science (print ISSN 0036-8075; online ISSN 1095-9203) is published weekly, except the last week in December, by the American Association for the Advancement of Science, 1200 New York Avenue NW, Washington, DC 20005.